Materials Letters 303 (2021) 130477

Contents lists available at ScienceDirect

Materials Letters

journal homepage: www.elsevier.com/locate/matlet

Experimental comparison of the effect of temperature on the vibrational and morphological properties of $Ni_xCo_{3-x}O_4$ nanostructures

Leydi Julieta Cardenas Flechas [a,*], Elena Xuriguera Martín [b], Jose Antonio Padilla Sanchez [b], Josep Ma Chimenos Ribera [b], Miryam Rincón Joya [c]

[a] Facultad de Ingeniería-Departamento de Ingeniería mecánica y mecatrónica, Universidad Nacional de Colombia-sede Bogotá, Colombia
[b] Departament de Ciència de Materials i Química Física, Universitat de Barcelona, Barcelona, Spain
[c] Departamento de Física, Universidad Nacional de Colombia-sede Bogotá, Colombia

ARTICLE INFO

Keywords:
Nickel doping
Vibrational properties
Thermal effect
Co_3O_4

ABSTRACT

This work presents the experimental comparison of the effect of temperature and nickel addition on the synthesis of $Ni_xCo_{3-x}O_4$ nanostructures x = 0.01, 0.04, 0.1, 0.16, using the sol–gel technique with final heat treatment at 600 °C and 800 °C. X-ray diffraction (XRD) analysis indicates the formation of pure Co_3O_4 at 600 °C and the appearance of an additional residual NiO phase at 800 °C. The presence of this phase evidences a deviation in the peaks of the diffraction angle to lower ones generated by the difference in ionic radii, which is related to the insertion of larger ions (Ni^{2+}) doped in the matrix of Co_3O_4. Scanning electron microscope (SEM) analysis indicates that there is a densification of the grains at higher temperatures, possibly associated with the thermal effect that generates greater interdiffusion. Fourier-transform infrared spectroscopy (FTIR) spectra show two main absorption bands with vibrations Co^{2+}¬O, Co^{3+}¬O and Ni¬O in 456 cm^{-1}. The effect of doping generates a displacement in the bands that are evident in the Raman analysis, where the vibrational mode A_{1g} at 600 °C is translated 28.07 cm^{-1}. The values of S_{BET} specific surface area indicate that as temperature increases, the surface area and volume of micropores decreases.

1. Introduction

Doping of transition metal compounds using various elements has proved to have synergistic effects in various properties and applications. Ag-Co_3O_4 was synthesized in the form of nanosheets and doping generated an increase in surface area minimization in the electron-hole process [1]. Xie et al. [2] explored the doping of Co_3O_4 with traces of metallic and non-metallic doping V and F. The synthesis of Fe/Co_3O_4 using different proportions of iron with a potential application for obtaining catalysts based on Co was carried out in [3,4,5]. The biomedical area is one of the most promising for the use of spinel ferrites. [6,7] Liu et al [8] doped Co_3O_4 with Ce and generated changes in textural properties that include pore structure and morphology, thus increasing specific surface area. Novel combinations have been studied, such as Co_3O_4 derived from ZIF-67 with In_2O_3, taking advantage of the p-n heterojunction of the metal oxide semiconductor [9]. There are other methods for the synthesis of oxide nanoparticles, including via solid state reaction [10] chemical deposition [11].

2. Materials and methods

The synthesis of $Ni_xCo_{3-x}O_4$ was carried out using the cobalt nitrate hexahydrate $Co(NO_3)_2{\cdot}6H_2O$ from Acros Organics brand with citric acid $C_6H_8O_7{\cdot}H_2O$ as precursors and in distilled water as solvent. The mixture was under stirring for 4 h at a temperature of 50 °C, subsequently, nickel nitrate hexahydrate ($N_2NiO_6{\cdot}6H_2O$) was added in percentages of 1, 4, 10 and 16 wt% To dehydrate the gel formed, the product was dried for 4 h at 80 °C. The product was then calcined in muffle furnace at 400 °C for 3 h. The final heat treatment was carried out on the samples obtained in a Carbolite brand oven at temperatures of 600 °C and 800 °C in air at the rate of 5 °C/min for 3 h. The structural analysis of the samples was performed with the PanAlytical X'Pert Pro powder diffractometer equipment with Cu-Kα radiation (k = 1.5418 Å), operating at 45 kV. Vibrational analysis of the samples was performed using Dispersive spectrometer Jobin-Yvon LabRam HR800 laser line 532 nm, laser power at sample: 0,5–5 mW and by Fourier-transform infrared spectroscopy (FTIR), on the Perkin-Elmer Spectrum Two Spectrometer. The

* Corresponding author.
E-mail addresses: ljcardenasf@unal.edu.co (L.J. Cardenas Flechas), xuriguera@ub.edu (E. Xuriguera Martín), japadilla@ub.edu (J.A. Padilla Sanchez), chimenos@ub.edu (J.M. Chimenos Ribera), mrinconj@unal.edu.co (M. Rincón Joya).

https://doi.org/10.1016/j.matlet.2021.130477
Received 1 July 2021; Received in revised form 12 July 2021; Accepted 14 July 2021
Available online 16 July 2021

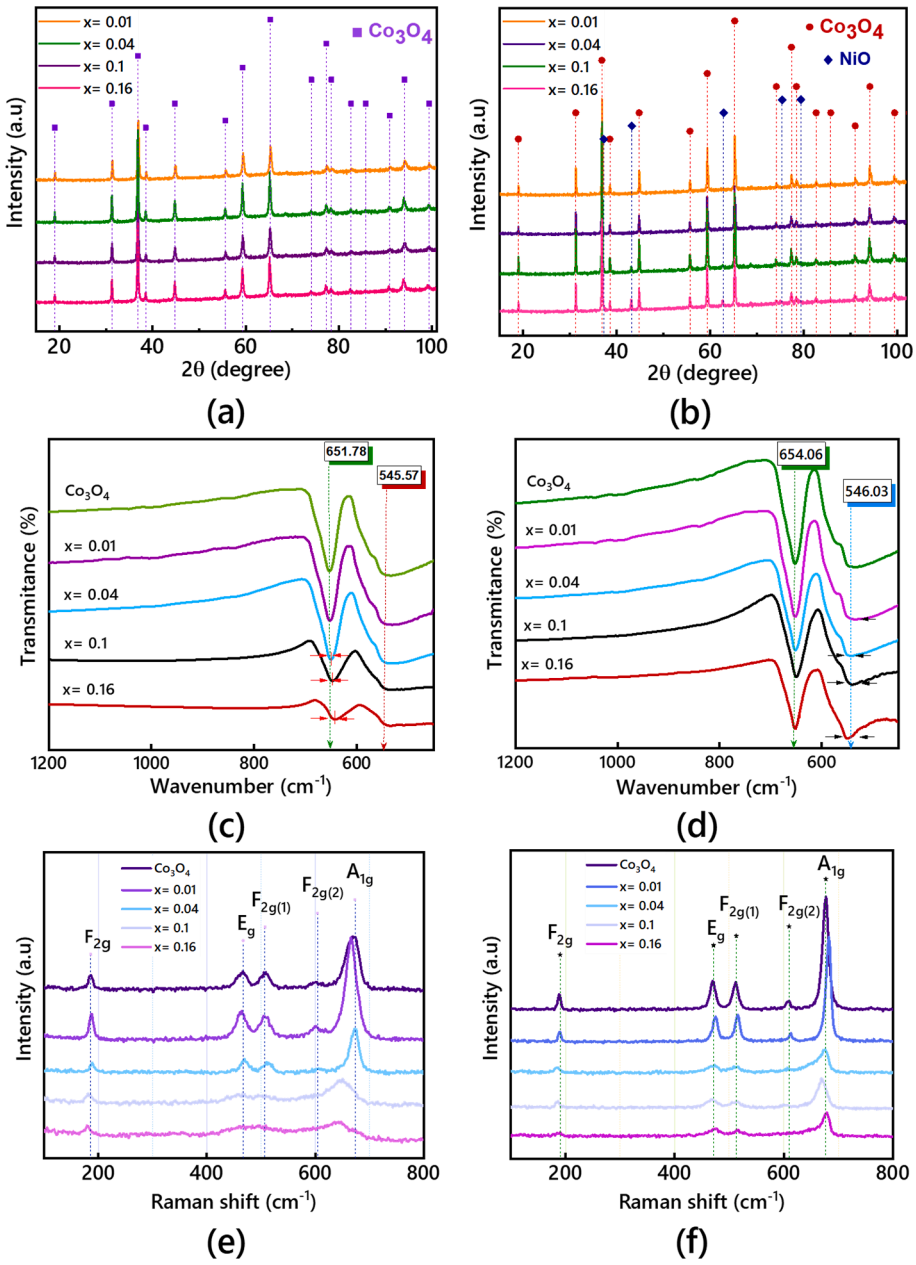

Fig. 1. Samples of $Ni_xCo_{3-x}O_4$ × = 0.01, 0.04, 0.10, 0.16 synthesized by the sol gel technique. XRD diffraction patterns: (a) 600 °C and (b) 800 °C. FTIR Spectrum: (c) 600 °C and (d) 800 °C. Raman Spectra: (e) 600 °C and (f) 800 °C.

morphology of the nanostructures was observed with the FESEMA-JEDL J-7100 scanning electron microscope (SEM). The surface area was determined by Brunauer-Emmett-Teller (BET) analysis of nitrogen adsorption–desorption isotherm using a Micromeritics TriStar 3000 V6.04A.

3. Results and discussion

Fig. 1a-b show the X-ray diffraction (XRD) patterns of $Ni_xCo_{3-x}O_4$ × = 0.01, 0.04, 0.1, 0.16 by means of the Sol-Gel technique with final heat treatment at (a) 600 °C and (b) 800 °C. At 600 °C the patterns show peaks at 18.9°, 31.2°, 36.8°, 38.5°, 44.8°, 55.6°, 59.3°, 65.2°, 74° and 77.3° with planes (111), (220), (311), (222), (400), (331), (422), (511), (440) and (533), respectively, that indicate the formation of the unique phase of Co_3O_4, Cod 01–073-1701, cubic crystal system characteristic of cobalt spinel [12]. The absence of peaks associated with the CoO phase reveals that the Co spinel oxide formed is pure [13]. In Fig. 1b, at 800 °C, the appearance of a residual phase additional to NiO-Co_3O_4 is observed in positions 2θ 37.2°, 43.2°, 62.8°, 75.3° and 79.3°, Cod 01–073-1523, with an increase in the intensity of the peaks due to the increase in temperature and the appearance of NiO [14].

The influence of Ni doping can be demonstrated by the deviation in the angle of the diffraction peaks to lower ones, caused by the insertion of larger doped ions in the Co_3O_4 matrix since the ionic radius of Ni^{2+} (0.69 Å) is greater than Co^{2+} (0.65 Å) and Co^{3+} (0.54 Å) [15,16]. The FTIR (Fig. 1c-d) spectra of the $Ni_xCo_{3-x}O_4$ samples are observed at (c) 600 °C and (d) 800 °C. At 600 °C, two main absorption bands υ_1 and υ_2 are observed at 653.6 and 545.94 cm^{-1}, which were attributed to the vibration of the metal–oxygen bond characteristic of Co_3O_4 [14]. A weak absorption is observed at 456 cm^{-1} and associated with the vibration of NiO [17]. The bands have a slight displacement when performing doping in the different percentages.

With x = 0.16, υ_1 is at 635.19 cm^{-1} while band υ_2 has a decrease in its peak shape. At 800 °C (Fig. 1d), the bands at 654.06 and 546.03 cm^{-1}

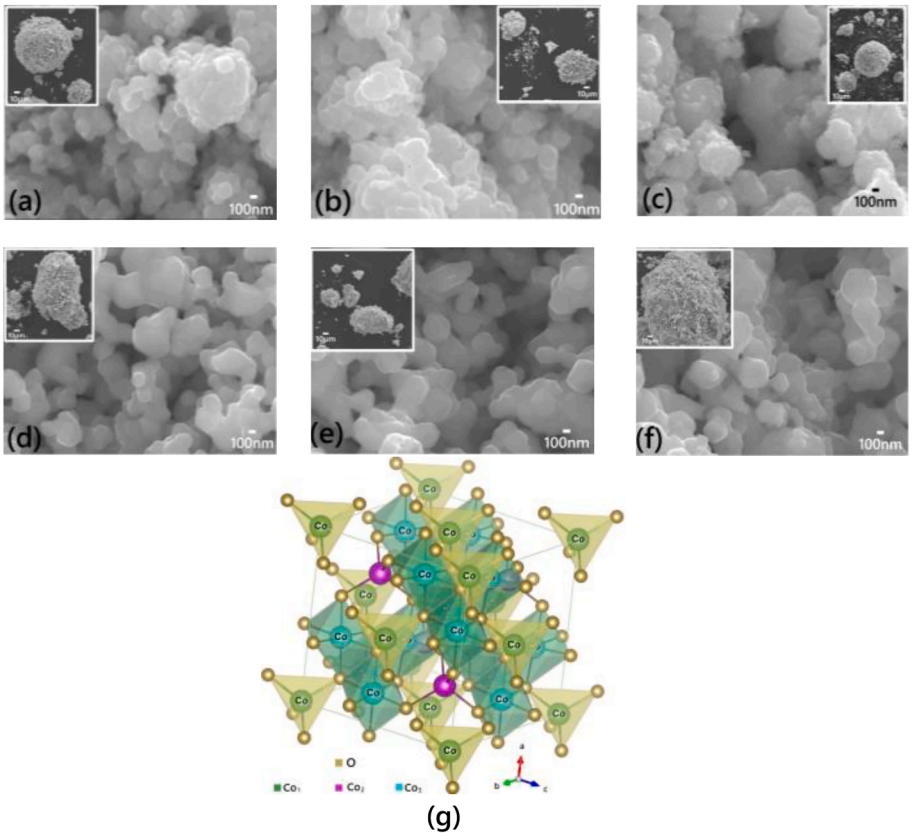

Fig. 2. FESEM images of $Ni_xCo_{3-x}O_4$ at 600 °C with (a) 0.01, (b) 0.04, (c) 0.16, and at 800 °C with (d) 0.01 (e) 0.04 (f) 0.16 and (g) Structural Co_3O_4 arrangement. Software Vesta.

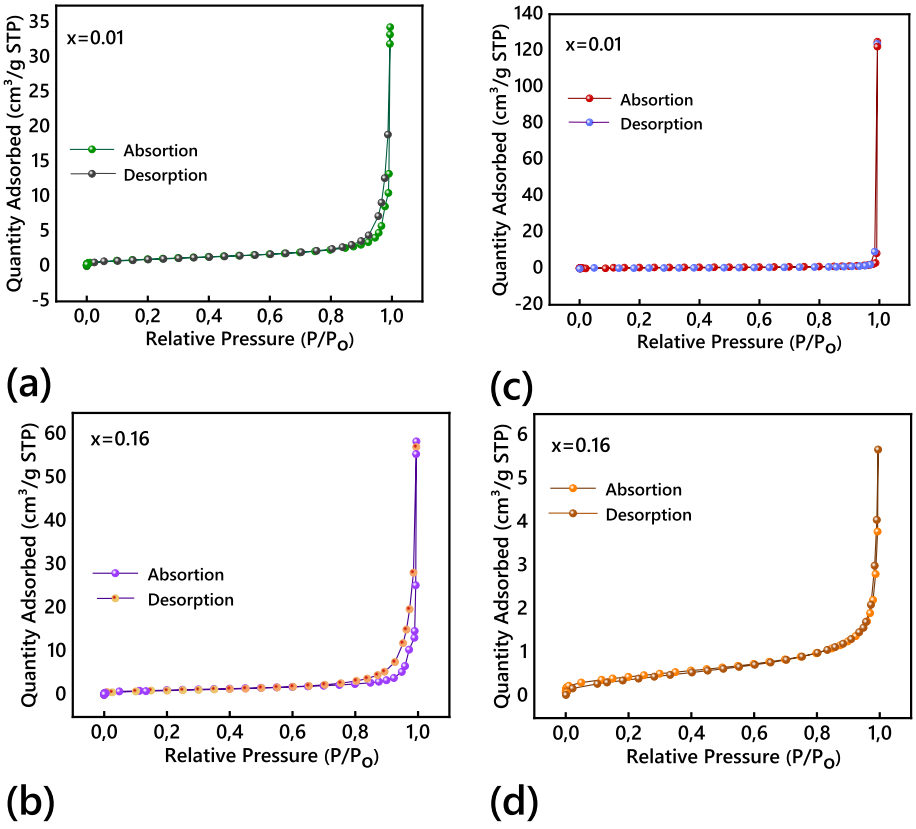

Fig. 3. N_2 adsorption desorption isotherms at 600 °C with (a) x = 0.01 and (b) x = 016, and at 800 °C with (c) x = 0.01 and (d) x = 0.16.

show a greater displacement depending on the doping point at υ_2, as well as the appearance of a band at 562.19 cm^{-1}. This band is related to the bending vibration modes of the Co_3O_4 and NiO [18], generated by the addition of nickel in the structure. The Raman spectra (Fig. 1e-f) are observed with five active Raman modes ($A_{1g} + E_g + 3F_{2g}$) that correspond to the Co_3O_4 phase in the spinel structure, where the incorporation of nickel causes the shift of Raman peaks towards numbers of lower waveforms with lower intensities.

For Ni concentrations of less than 4%, the Raman spectra are similar for temperatures of 600 °C and 800 °C, with higher crystallinity at 800 °C due to the intensity of the larger and narrower peaks. For Ni concentrations greater than 4%, the Raman modes broaden, indicating amorphization in the samples or a spinel lattice with a secondary phase. The increase in Ni concentration deteriorates the spinel network, hence the Ni concentration cannot be greater than 4%.

Fig. 2a-f show the morphology of the $Ni_xCo_{3-x}O_4$ samples examined with Field emission scanning electron microscopy (FESEM) analysis, where semi-octahedral and irregular nanostructures are observed, with an agglomeration without specific arrangement [17]. An agglomerated structure has proved to be advantageous over non-agglomerated nanoparticles [18]. At 800 °C densification of the grains is observed and it can be associated with the thermal effect that generates greater interdiffusion. Depending on the type of synthesis, as well as on the reagents used and reaction times, the nanoparticles will have different shapes and distributions. According to Majid et al. [19], due to the concentration of nickel in cobalt ions, the location of anions and cations changes in octahedral sites and parameters, such as dislocation density, and oxygen position changes with the increase in the concentration of Ni^{2+} in cobalt ferrites. In the structure of cobalt tetraoxide, when nickel is incorporated, it preferably substitutes the octahedral sites of Co^{3+} through stabilization at sites $^{2+}$ and $^{3+}$ [20] as shown in Fig. 2g.

Fig. 3a-d show the adsorption–desorption isotherms of N_2 for the samples obtained at 600 °C with (a) 1% and (b) 16%, and at 800 °C with (c) 1% (d) 16%. According to the IUPAC classification, all isotherms are classified as type IV, which is associated with a disordered mesoporous structure. [21] The P/P_0 less than 0.5 values of the isotherms suggest micropores in the samples, confirmed by the H3 hysteresis loops [16] with which the samples are identified. The values of the S_{BET} specific surface area indicate that, as the temperature increases, the surface area and volume of micropores decreased, since at 800 °C the values are in the range of 1.63 $m^2 \cdot g^{-1}$ to 1.82 $m^2 \cdot g^{-1}$, while at 600 °C the highest value obtained by the sample with nickel doping x = 0.04 was 4.34 $m^2 \cdot g^{-1}$ with a pore volume of 0.05 $cm^3 \cdot g^{-1}$. This behaviour can be attributed to densification and sintering that increased with the calcination temperature as indicated [14].

4. Conclusions

The objective of the research was to evaluate the effect of nickel addition on nanostructures of $Ni_xCo_{3-x}O_4$ with different concentrations of Ni and final thermal treatment at 600 °C and 800 °C. Results of XRD show that the nickel addition at 800 °C produces the appearance of a residual phase of NiO. Results FTIR indicate vibrations of $Co^{2+}\neg O$ and $Co^{3+}\neg O$ in the structure of Co_3O_4 as well as Ni¬O, produced by doping. Raman measurements evidenced that the peaks decrease the intensity and augment widening with the increase in Ni concentration of more than 4%, thus indicating the presence of a residual phase of NiO. Raman modes are narrower and more intense at 800 °C and concentrations lower than 4%, which evidences more crystallinity in the material. S_{BET} values show that the increase in temperature diminishes the surface area and volume, possibly due to densification.

CRediT authorship contribution statement

Leydi Julieta Cardenas Flechas: Investigation, Conceptualization, Writing, Methodology. **Elena Xuriguera Martín:** Methodology, Supervision, Resources. **Jose Antonio Padilla Sanchez:** Investigation, Editing. **Josep Ma. Chimenos Ribera:** Conceptualization, Editing, Resources. **Miryam Rincón Joya:** Methodology, Investigation, Supervision.

Declaration of Competing Interest

The authors declare that they have no known competing financial interests or personal relationships that could have appeared to influence the work reported in this paper.

Acknowledgments

The authors thank Universidad Nacional de Colombia - Campus Bogotá, Fundación Carolina-SEGIB and the Centres Científics i Tecnològics (CCiT) of the Universitat de Barcelona, for the support in the research stay in 2021.

References

[1] M. Aadil, S. Zulfiqar, M.F. Warsi, P.O. Agboola, I. Shakir, M. Shahid, N. Al-Khalli, Ceram. Int. 47 (7) (2021) 9806–9817, https://doi.org/10.1016/j.ceramint.2020.12.121.
[2] J. Xie, R.Y. Fan, J.Y. Fu, Y.N. Zhen, M.X. Li, H.J. Liu, B. Dong, Int. J. Hydrog. Energy 46 (38) (2021) 19962–19970, https://doi.org/10.1016/j.ijhydene.2021.03.141.
[3] Z. Li, J. Kang, Y. Tang, C. Jin, H. Luo, S. Li, C. Lv, J. Alloy. Compd. 858 (2021), 157739, https://doi.org/10.1016/j.jallcom.2020.157739.
[4] D.A. Vinnik, V.E. Zhivulin, D.P. Sherstyuk, A.Y. Starikov, P.A. Zuzina, S. A. Gudkova, D.A. Zherebtsov, K.N. Rozanov, S.V. Trukhanov, K.A. Astapovich, V. A. Turchenko, A.S.B. Sombra, D. Zhou, R.B. Jotania, C. Singh, A.V. Trukhanov, Mater. Today Chem. 20 (2021), 100460, https://doi.org/10.1016/j.mtchem.2021.100460.
[5] M.V. Zdorovets, A.L. Kozlovskiy, D.I. Shlimas, D.B. Borgekov, J. Mater. Sci.: Mater. Electron. (2021), https://doi.org/10.1007/s10854-021-06226-5.
[6] D.I. Tishkevich, I.V. Korolkov, A.L. Kozlovskiy, M. Anisovich, D.A. Vinnik, A. E. Ermekova, A.I. Vorobjova, E.E. Shumskaya, T.I. Zubar, S.V. Trukhanov, M. V. Zdorovets, A.V. Trukhanov, J. Alloy. Compd. 797 (2019) 573–581, https://doi.org/10.1016/j.jallcom.2019.05.075.
[7] M.A. Almessiere, A.V. Trukhanov, F.A. Khan, Y. Slimani, N. Tashkandi, V. A. Turchenko, T.I. Zubar, D.I. Tishkevich, S.V. Trukhanov, L.V. Panina, A. Baykal, Ceram. Int. 46 (2020) 7346–7354, https://doi.org/10.1016/j.ceramint.2019.11.230.
[8] W. Liu, J. Fan, Z. Song, X. Zhang, Appl. Organomet. Chem. 35 (1) (2021), e6053, https://doi.org/10.1002/aoc.6053.
[9] D. Han, X. Li, F. Zhang, F. Gu, Z. Wang, Sensor Actuat B-Chem. 340 (2021), 129990, https://doi.org/10.1016/j.snb.2021.129990.
[10] D.A. Vinnik, V.E. Zhivulin, D.P. Sherstyuk, A.Y. Starikov, P.A. Zezyulina, S. A. Gudkova, D.A. Zherebtsov, K.N. Rozanov, S.V. Trukhanov, K.A. Astapovich, A.S. B. Sombra, D. Zhou, R.B. Jotania, C. Singh, A.V. Trukhanov, J. Mater. Chem. C 9 (2021) 5425–5436, https://doi.org/10.1039/D0TC05692H.
[11] A. Kozlovskiy, K. Egizbek, M.V. Zdorovets, M. Ibragimova, A. Shumskaya, A. A. Rogachev, Z.V. Ignatovich, K. Kadyrzhanov, Sensors 20 (2020) 4851, https://doi.org/10.3390/s20174.
[12] K. Lakshmi, S. Revathi, Mater. Charact. 177 (2021), 111160, https://doi.org/10.1016/j.matchar.2021.111160.
[13] A.K. Swaghatha, L. Cindrella, Polym. J. 53 (2021) 679–693, https://doi.org/10.1038/s41428-021-00466-2.
[14] B. Abu-Zied, S.A. Soliman, S.E. Abdellah, Chin. J. Catal. 35 (2014) 1105–1112, https://doi.org/10.1016/S1872-2067(14)60058-9.
[15] L. Guo, F. Chen, N. Xie, C. Wang, X. Kou, Y. Sun, G. Lu, J. Colloid Interface Sci. 528 (2018) 53–62, https://doi.org/10.1016/j.jcis.2018.05.089.
[16] P. Cheng, F. Dang, Y. Wang, J. Gao, L. Xu, C. Wang, B. Liu, Sensor Actuat. B Chem. 328 (2021), 129028, https://doi.org/10.1016/j.snb.2020.129028.
[17] G.A. Babu, G. Ravi, Y. Hayakawa, J. Appl. Phys. 119 (2015) 219–232, https://doi.org/10.1007/s00339-014-8951-9.
[18] J. Gupta, A. Ahmed, Phys. B: Condens. Matter. 599 (2020), 412383, https://doi.org/10.1016/j.physb.2020.412383.
[19] F. Majid, I. Wahid, S. Ata, I. Bibi, M. Ali, A. Malik, A. Nazir, Mater. Chem. Phys. 264 (2021), 124451, https://doi.org/10.1016/j.matchemphys.2021.124451.
[20] L. Cardenas-Flechas, A.M. Raba, M. Rincón-Joya, Revista Dyna 87 (213) (2020) 184–191, https://doi.org/10.15446/dyna.v87n213.84410.
[21] L.F. Oton, A.C. Oliveira, S. Tehuacanero-Cuapa, G.D. Saraiva, F.F. de Sousa, A. Campos, J.R. Bezerra, J. Mol. Catal. 496 (2020), 111186, https://doi.org/10.1016/j.mcat.2020.111186.